Resonant Modes in Exotic Compact Objects

Yasmeen Asali,[1] Peter Tsun-Ho Pang,[2] and Chris van den Broeck[2]

[1] *Columbia University, New York, New York 10027, USA*
[2] *Nikhef, Science Park 105, 1098 XG Amsterdam, Netherlands*

Resonantly excited quasinormal modes in compact binary mergers will result in a phase jump in the gravitational waveform as energy is absorbed by the resonance. This feature is evident in binary neutron star mergers, and this work explores similar resonant mode features in exotic compact object binaries in the black hole mass range. We show that resonances with resultant phase shifts or order unity or larger can produce detectable events using a background-foreground approach for model selection.

I. INTRODUCTION

It has been shown that resonant modes can be excited in binary neutron star systems [2]. These Rossby modes are catalyzed by tidal interactions and can cause inspiral to quicken due to a phase shift in the gravitational wave phase. It is reasonable to assume a similar effect can occur from other types of resonances that pull energy from the system. In this work we consider the plausibility and detectability of such resonances in Exotic Compact Objects (ECOs). ECOs are horizonless objects with densities comparable to neutron stars or black holes and potentially beyond-the-standard-model features. Mergers containing at least one ECO may be differentiated from binary black hole systems by the presence of resonant modes during inspiral.

In Sec. 2 we outline the theoretical motivation for resonant mode searches in ECOs. Sec. 3 explains the methodology and Sec. 4 details the results of our study and Sec. 5 presents our discussion of the results.

II. THEORETICAL MOTIVATION

There are a number of ECO models that predict phenomena beyond general relativity which may cause detectable effects on the gravitational waveform. A common ECO model considers some "closeness" parameter ϵ that quantifies how similar ECO spacetime is to that of a BH. In Cardoso et al. (2019), ϵ is defined as follows:

$$r_0 = 2M(1+\epsilon) \tag{1}$$

where ϵ is an additional shell around a horizonless, BH-like object, and as $\epsilon \to 0$, BH spacetime is recovered [1]. This "shell" will create a cavity between the hard inner boundary at r_0 and photonsphere. One can imagine this as a sort of Fabry-Perot cavity, and certain resonant gravitational wave frequencies will cause spacetime itself to resonate inside this cavity. Ongoing work that is not yet published has shown that reasonable resonant frequencies occurring before the binary system merges where $f_0 < f_{\rm ISCO}$ will not produce a phase shift in the gravitational wave within the range of detectability by Advanced LIGO.

A boson star (BS) is another theorized ECO satisfying the Einstein-Klein-Gordon equations. As described in Macedo et al. (2013), BS models are classified by scalar potential and predict a wide range of masses [3]. Three popular BS models are mini, massive, and solitonic boson stars. Mini BSs have a maximum mass described by the Kaup limit $M_{max} \approx 0.633 m_p^2/\mu$ where m_p denotes the Planck mass and μ is the scalar field mass [3]. For typical values of μ, the maximum mass of a mini-BS can be significantly small than the Chandrasekhar limit. At the other extreme, the solitonic BS model allows for masses of the same order as supermassive objects where $M \sim 10^6 M_\odot$. It is plausible to have a massive BS meeting the condition that resonance occurs at $f_0 < f_{\rm ISCO}$, and we show it may induce a phase shift that can be of order unity or greater.

Resonant Modes in Boson Stars

As in NS mergers, for some binary BS configurations quasinormal modes (QNMs) can be excited during inspiral, unlike the BH case where QNMs are only excited as the system merges. The affect of such resonant modes on the gravitational waveform was shown in Flanagan et al. (2007) to generally take the following form:

$$\Phi(t) = \begin{cases} \Phi_{pp}(t) & \text{if } t < t_0 \\ \Phi_{pp}(t+\Delta t) - \Delta\Phi & \text{if } t \geq t_0 \end{cases} \tag{2}$$

where the gravitational wave phase $\Phi(t)$ during inspiral deviates from the point particle phase $\Phi_{pp}(t)$ by a shift in phase and time once the resonance occurs at t_0 [2]. The resonance will cause an overall phase shift and a time shift in the gravitational wave signal, and when this Δt is sufficiently small, one can approximate $\frac{\Delta\Phi}{\Delta t}$ as a derivative such that:

$$\Delta\Phi = \dot{\Phi}_{pp}(t_0)\Delta t \tag{3}$$

This expression can be substituted into the previous equation for the case where $t \geq t_0$, and with a Taylor expansion one can produce the following:

$$\Phi(t) = \Phi_{pp}(t) + \dot{\Phi}_{pp}(t)\Delta t - \dot{\Phi}_{pp}(t_0)\Delta t \tag{4}$$

The gravitational wave frequency will be twice the orbital frequency, so $\dot{\Phi}_{pp} = 2\omega$. Using this relationship we can also say $\Delta t = \frac{\Delta\Phi}{2\omega(t_0)}$. Substituting these values in and simplifying produces this expression:

$$\Phi(t) = \Phi_{pp}(t) + \left[\frac{\omega(t)}{\omega(t_0)} - 1\right]\Delta\Phi \tag{5}$$

In the frequency domain, this can be rewritten as:

$$\phi(f) = \phi_{pp}(f) + [\frac{f}{f_0} - 1]\Delta\phi \tag{6}$$

The gravitational wave phase ϕ is described by the point particle phase ϕ_{pp} and some additional shift due to resonant excitation, where f is the gravitational wave frequency, f_0 is the resonant frequency, and $\Delta\phi$ is the resonant mode phase shift. In practice, both objects in the binary system may experience resonant excitation. The above equation can be modified to account for this in the following way:

$$\phi(f) = \phi_{pp}(f) + (\frac{f}{f_{01}} - 1)\Delta\phi_{01} + (\frac{f}{f_{02}} - 1)\Delta\phi_{02} \tag{7}$$

where each of the two objects may contribute its own phase shift. It is worth noting that this equation is only valid in the case where $f \geq f_{01}\text{and}f_{02}$. If the gravitational wave frequency only passes the resonant frequency of one of the objects, only that object will undergo resonant excitation and thus the equation will only have one additional phase shift term. Fig. 1 shows how this effect will manifest in the waveform. The BBH waveform is fully described by point particle evolution, ϕ_{pp}, and the pictured ECO waveform has an exaggerated phase shift for clarity. The two dotted vertical lines show the time when resonance occurs for each object. The dephasing of the ECO waveform begins prior to the time of resonance, evident by the splitting of the two lines at around 3.4 seconds, due to the fact that resonance does not occur instantaneously but rather it gradually begins as the $f \to f_0$.

We can estimate the phase shift induced by a massive BS from the fundamental $l = m = 2$ mode with the following formula:

$$\Delta\phi = \frac{\Delta E}{\dot{E}_{pp} t_{orb}} \gtrapprox 1 \tag{8}$$

where ΔE is the energy emitted during resonance and $\dot{E}_{pp}$ refers to rate of energy loss during point particle inspiral. The energy emitted during resonance can be calculated the following way:

$$\Delta E = \dot{E}_{gw} t_{res} \tag{9}$$

for the energy transferred by the gravitational wave $\dot{E}_{gw}$ during the duration of resonance t_{res}. Using the results of Macedo et al. (2013), one can estimate this phase shift to be of order unity or larger for resonant modes occurring before merger in massive boson star inspirals [3].

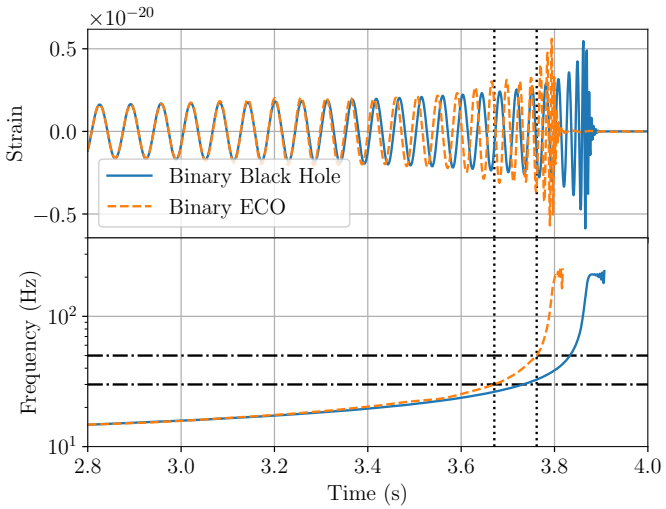

FIG. 1: Top Panel: BBH and ECO time domain waveforms. Bottom Panel: BBH and ECO chirp signals in frequency versus time.

III. METHODOLOGY

We perform a mock data analysis to test the detectability of resonant modes in ECOs by Advanced LIGO / Virgo. Bayesian analysis methods were used on simulated signals to determine if ECO injections could be statistically differentiated from BBH injections.

Bayesian Analysis

Consider a hypothesis H that provides a description of the data d given a known parameter θ. The plausibility of the data d is dependent on a number of values, namely the likelihood function $p(d|\theta, H, I)$, the prior probability $p(\theta|H, I)$, and the evidence $p(d|H, I)$, where I represents the state of knowledge prior to the experiment.

Through Bayes' theorem, the posterior probability of a given parameter θ can be expressed in the following way:

$$p(\theta|d, H, I) = \frac{p(d|\theta, H, I)p(\theta|H, I)}{p(d|H, I)} \tag{10}$$

The likelihood $p(d|\theta, H, I)$ refers to the probability of the hypothesis describing the data. The prior $p(\theta|H, I)$ represents the probability of the parameter given your hypothesis and I. Essentially, it is the state of knowledge of the parameter θ before the experiment is conducted. We use simulated gaussian noise, so the logarithm of the likliehood function can be given by:

$$\log p(d|\theta) \propto -\frac{1}{2}\langle d - h(\theta)|d - h(\theta)\rangle \tag{11}$$

where the model given by your hypothesis is denoted by h. This inner product for gravitational wave data is given

by the following integral over the frequency bandwidth of the detector:

$$\langle a|b\rangle = 4Re\int_{f_{low}}^{f_{high}} \frac{\tilde{a}(f)\tilde{b}^*(f)}{S_n(f)}df \tag{12}$$

where S_n is the power spectral density, and thus your likelihood is weighted by the detector sensitivity.

The evidence $p(d|H,I)$ is given by the likelihood for one parameter, weighted by the prior on that parameter, and then marginalized over all parameters. It can be expressed the following way:

$$p(d|H,I) = \int p(d|\theta,H,I)p(\theta|H,I)d\theta \tag{13}$$

This expression shows that the evidence is independent of the value of any given parameter θ. For the purposes of hypothesis testing and model selection discussed in Sec. 2.b, the evidence is crucial and we will come back to it. However, for the purposes of parameter estimation and recovering some posterior distribution for θ, the evidence is unimportant. Therefore, the posterior can be rewritten in the following way as a proportionality:

$$p(\theta|d,H,I) \propto p(d|\theta,H,I)p(\theta|H,I) \tag{14}$$

One can express this distribution is slightly different and more straightforward notation:

$$\mathcal{P}(\theta) \propto \mathcal{L}(\theta)\pi(\theta) \tag{15}$$

where $\mathcal{P}(\theta)$ is the posterior of some parameter θ, $\mathcal{L}(\theta)$ is the likelihood function, and $\pi(\theta)$ is the prior. In this notation, the evidence is expressed as Z though it is not included in equation 15 as it is parameter independent.

Hypothesis Testing

Hypothesis testing, also referred to as model selection, is a method for determining the viability of different models by comparing the ratio of evidences. This ratio is denoted by the Bayes factor $\mathcal{B}$, and is defined in the following way for two hypotheses X and Y:

$$\mathcal{B}^X_Y = \frac{Z_X}{Z_Y} \tag{16}$$

where the evidence Z is described by

One can construct a Bayes factor $\mathcal{B}^{\rm ECO}_{\rm BBH}$ which compares the validity of the ECO model against a purely BBH model against a set of gravitational wave detections. A larger value will imply a better fit given the ECO model, and conversely a smaller Bayes factor will support the BBH model. Each nested sampling run with `LALInference` will return a Bayes factor weighing the signal to noise, $\mathcal{B}^{\rm S}_{\rm N}$. One can then compare two different hypotheses by taking the difference between the respective Bayes factors in the following way:

$$\log(\mathcal{B}^{\rm ECO}_{\rm BBH}) = \log\left(\mathcal{B}^{\rm S}_{\rm N(ECO)}\right) - \log\left(\mathcal{B}^{\rm S}_{\rm N(BBH)}\right) \tag{17}$$

Note that we switch to logarithm notation here as it is somewhat easier to work with and provides a more reasonable scale. Here $\mathcal{B}^{\rm S}_{\rm N(ECO)}$ refers to the case where parameters are recovered assuming an ECO waveform with resonant modes, and similar notation denotes BBH recovery.

Theoretically, this measure alone should be enough to weigh the degree of belief in the ECO hypothesis; however, the level of noise in the case of gravitational wave data from advanced detectors can easily mask a signal. False detections can arise from noise that mimics ECO-like features, but can be avoided by constructing background and foreground distributions. The background distribution signifies the case where waveforms described by GR with no resonant modes were injected, so the BBH hypothesis should better describe the data. Similarly, the foreground distribution is constructed by injecting ECO waveforms with resonant mode features. Furthermore, constructing these two distributions is necessary as the ECO and BBH hypotheses do not provide an exhaustive set of predicted waveforms.

Implementation

Resonant mode effects for each object were added into the waveform generation function of `LALSimulation` as a new version within IMRPhenomPv2. For two non-identical objects, the corresponding resonant frequencies will be different so once one of the two reaches the required resonant frequency the first phase shift is inserted. As the second object meets its respective resonant frequency, the second phase shift is inserted. If the resonant frequencies for one or both of the objects occurs after the innermost stable circular orbit frequency ($f_{\rm ISCO}$) then no phase shift is added.

Four new variables were added as free parameters into `LALInference`. Specifically, these parameters were the phase shifts of the two objects, the higher of the two resonant frequencies, and the ratio between the two resonant frequencies. By sampling over the higher frequency and frequency ratio, we avoid artificial bimodality in the posterior distributions that can occur from the algorithm trying to recover both of the frequency peaks. A flat prior is used for sampling over all parameters.

Nested sampling performs both model selection and parameter estimation as it computes the evidence integral and returns samples from the posterior distribution. A thorough explanation of the nested sampling algorithm used in `LALInference` can be found in Ref. [4].

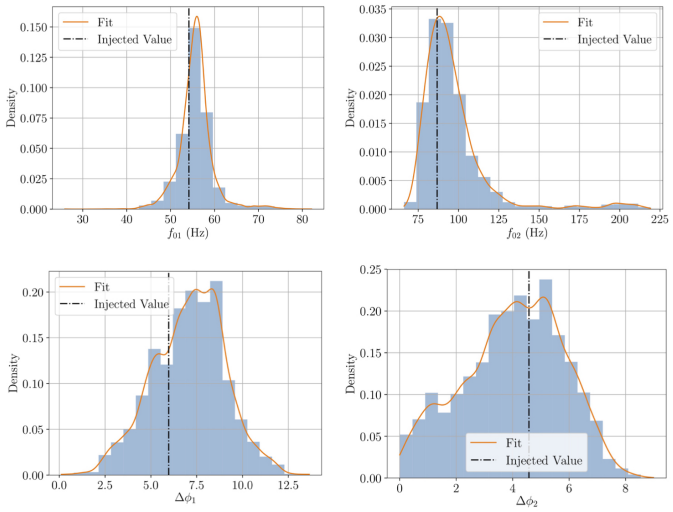

FIG. 2: Example parameter estimation result showing posterior distributions for resonant mode parameters for one event

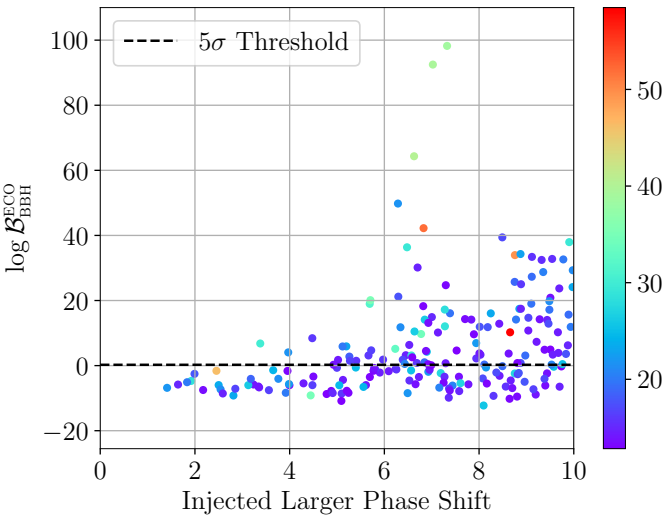

FIG. 3: Bayes factor against the larger of the two injected phase shifts for events in the foreground distribution, colored by network SNR

IV. RESULTS

Our simulation consisted of 200 ECO injections and 200 BBH injections for comparison. The injected parameters for the mock ECO data were set in the following ways. Frequency and phase shift were injected for both objects in the binary using a uniform distribution between $[20, 110]$ Hz and $[0, 10]$ radians respectively. The frequency bounds were set by the lower frequency limit for the detectors and the maximum f_{ISCO} given the minimum possible masses. Component masses were injected uniformly between $[20, 30]M_{\odot}$. SNRs were injected for an expected network SNR in the range $[12, 60]$ and distributed in volume, which corresponds to $\frac{1}{\mathrm{SNR}^3}$. ECO recovery priors allowed for frequencies ranging from $[20, 220]$ Hz, phases ranging from $[0,\ 100]$, and masses from $[10, 40]M_{\odot}$.

An example of the parameter estimation results for ECO recovery are shown in Fig. 2 for one of the 200 injections. This particular injection had a network SNR of 16.18 and a $\log\left(\mathcal{B}^{\mathrm{ECO}}_{\mathrm{BBH}}\right) = 1.836$. This is well above the threshold for a false alarm probability of 5σ, which corresponds to a $\log\left(\mathcal{B}^{\mathrm{ECO}}_{\mathrm{BBH}}\right) \approx 0.2$. Fig. X displays how each of the resonant mode parameters were well recovered, evident by the fact the injected values are well within the posterior distributions.

We assess detectability using a background-foreground approach, where the threshold above which an event can be distinguished from the background corresponds to a false alarm probability (FAP) of 5σ. Fig. 3 plots all 200 injected foreground events colored by network SNR. The larger of the two injected phase shifts is plotted against the $\log\left(\mathcal{B}^{\mathrm{ECO}}_{\mathrm{BBH}}\right)$. As one would expect, the number of events above the 5σ detectability threshold increases with larger phase shifts and SNRs, since the deviations from BBH waveforms become more evident. Additionally, events with phase shifts as low as 3.5 may be detectable given sufficient SNR.

Fig. 4 shows the distributions of the Bayes factor for the ECO hypothesis over the BBH hypothesis where the foreground distribution has waveforms injected with resonant modes and the background has injections without resonant modes. It is evident that the background distribution is better described by the BBH hypothesis as it is largely negative. Similarly, the foreground case uses injected waveforms with resonant modes, and as expected the ECO hypothesis is favored in recovery. The two distributions are fairly separated, and a sizable amount of foreground injections lie well outside of the background distribution and above the 5σ detectability threshold of 0.2.

The efficiency describes the amount of the foreground distribution that is above the threshold, and it can be pushed using the cataloging method described in Li (2013). Catalogs are constructed by taking random samples from the full injection set and essentially averaging over the Bayes factors. This method was employed on our data with a catalog size of 10 events, and the results are plotted in Fig. 5. The efficiency is pushed to 100% as the foreground distribution is clearly separated from the background.

V. DISCUSSION

ECOs may exhibit resonance during inspiral, and boson stars are particularly good candidates for exhibiting

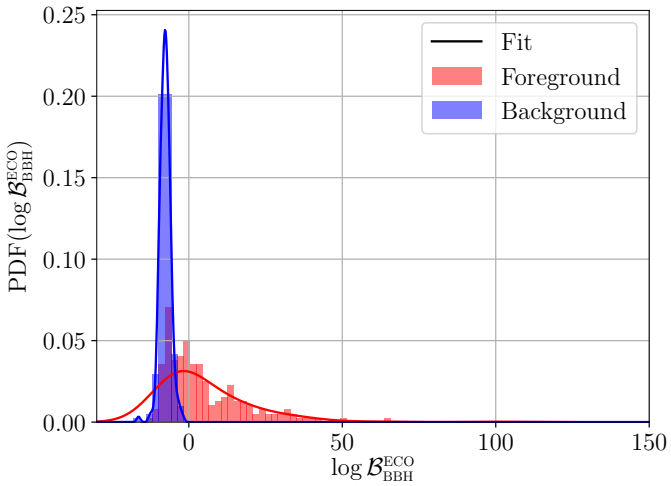

FIG. 4: The background and foreground distributions of the Bayes factor of the ECO over BBH hypotheses, with gaussian KDE fits

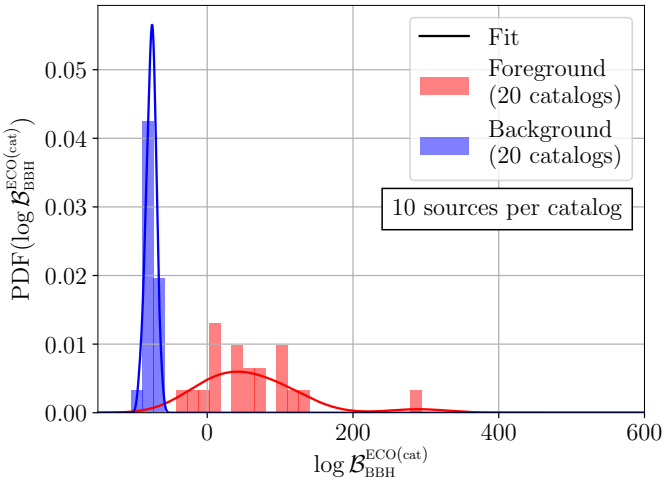

FIG. 5: The cataloged background and foreground distributions using 10 sources per catalog, with gaussian KDE fits

detectable resonance features. With phase shifts of order unity or larger, boson star resonances

This project is ongoing and future work includes repeating this analysis on real data with the actual detector sensitivity. Additionally, events that are marginally detectable with this method may not be detected by standard parameterized tests of GR.

ACKNOWLEDGMENTS

I'm grateful to Peter and Chris for being amazing supervisors and mentors, and to the program coordinators for all of their hard work. Additionally, many thanks to the collaborators who aided this work and provided valuable lessons. I would also like to thank the University of Florida and National Science Foundation for the opportunity and the National Dutch Institute for Subatomic Physics for hosting me.

[1] Cardoso, Vitor, del Rio, Adrian, & Kimura, Masashi. 2019. Distinguishing black holes from horizonless objects through the excitation of resonances during inspiral. *arxiv e-prints*, Jul, arXiv:1907.01561.

[2] Flanagan, Éanna É., & Racine, Étienne. 2007. Gravitomagnetic resonant excitation of Rossby modes in coalescing neutron star binaries. Phys. Rev. D, **75**(4), 044001.

[3] Macedo, Caio F. B., Pani, Paolo, Cardoso, Vitor, & Crispino, Luís C. B. 2013. Astrophysical signatures of boson stars: Quasinormal modes and inspiral resonances. Phys. Rev. D, **88**(6), 064046.

[4] Veitch, J., Raymond, V., Farr, B., Farr, W., Graff, P., Vitale, S., Aylott, B., Blackburn, K., Christensen, N., Coughlin, M., Del Pozzo, W., Feroz, F., Gair, J., Haster, C. J., Kalogera, V., Littenberg, T., Mandel, I., O'Shaughnessy, R., Pitkin, M., Rodriguez, C., Röver, C., Sidery, T., Smith, R., Van Der Sluys, M., Vecchio, A., Vousden, W., & Wade, L. 2015. Parameter estimation for compact binaries with ground-based gravitational-wave observations using the LALInference software library. Phys. Rev. D, **91**(4), 042003.